

# A Comparison of Neural Networks and Fuzzy Inference Systems for the Identification of Magnetic Disturbances in Mobile Robot Localization

Massimo Stefanoni<sup>1</sup>, Márta Takács<sup>2</sup>, Ákos Odry<sup>3,4</sup>,  
Peter Sarcevic<sup>3</sup>

<sup>1</sup> Doctoral School of Applied Informatics and Applied Mathematics,  
Obuda University, Bécsi 96/B, H-1034 Budapest, Hungary,  
massimo.stefanoni@uni-obuda.hu

<sup>2</sup> John von Neumann Faculty of Informatics, Obuda University, Bécsi 96/B,  
H-1034 Budapest, Hungary, takacs.marta@nik.uni-obuda.hu

<sup>3</sup> Department of Mechatronics and Automation, Faculty of Engineering,  
University of Szeged, Mars tér 7, H-6724 Szeged, Hungary,  
odrya@mk.u-szeged.hu, sarcevic@mk.u-szeged.hu

<sup>4</sup> Institute of Informatics, University of Dunaújváros,  
Táncsics Mihály u. 1/A, H-2400 Dunaújváros, Hungary,  
odrya@uniduna.hu

---

*Abstract: Three-axis magnetometers are widely used in the field of localization in both outdoor and indoor environments. However, magnetic field measurements are disturbed by the presence of metallic objects due to the soft and hard-iron effects. To neglect these effects, a compensation technique is required, and, in this article, different solutions are proposed and evaluated to compensate for the disturbance effects of metallic objects with known fingerprints. These techniques exploit an already presented concept in the literature that is able to provide the compensation values of a known detected object using the distance and angle as inputs to a single hidden layer Artificial Neural Network (ANN). In this work, unlike the original proposal, each new presented technique exploits a modified or a different soft computing tool, such as a double hidden ANN, a Fuzzy Inference System (FIS), and an Adaptive Neural FIS (ANFIS). The techniques were tested with real measurements of three different objects, and the performances of the techniques were compared using the maximum errors, the Mean Absolute Errors (MAEs) of every single component, and the total MAEs. Overall, among them, only the ANN techniques and the ANFIS provided acceptable results. More precisely, the former provided maximum errors in the range between 0.3  $\mu\text{T}$  and 3.8  $\mu\text{T}$ , and MAEs in the order of 0.07  $\mu\text{T}$ , whereas the latter was the one that provided the best performance, giving a residual maximum error in the order of  $10^{-3}$   $\mu\text{T}$  and an MAE in the order of  $10^{-5}$   $\mu\text{T}$ .*

*Keywords: magnetometer; localization; disturbance compensation; mobile robot; neural network; fuzzy inference system; adaptive neuro-fuzzy inference system*

---

## 1 Introduction

Magnetometers are widely used in the field of both localization and tracking, and are adopted in several applications such as permanent magnet localization [1] [2], underwater object tracking [3], creation of magnetic maps [4], localization of pedestrians [5], smartphone-based indoor positioning [6], indoor navigation systems [7], tracking of vehicles [8], tracking of metallic targets [9], magnetic fingerprint-based robot localization [10] [11], enhanced dead-reckoning localization method for skid-steering robots [12], or detection of unexploded ordnance [13].

The magnetic data can be fused with data from other sensors, like gyroscopes and accelerometers, to estimate the robot pose [14] or to estimate the velocity [15]. It can also be combined with data from other systems, such as the Global Navigation Satellite System (GNSS) [16], or with radio modules [17] [18].

Three-axis magnetometers are used in both outdoor and indoor environments. In the former, the sensor is used as a compass and provides the orientation with respect to the global localization frame [19]; moreover, outdoor measurements of the geomagnetic field are usually not affected by disturbances, and magnetometers can be used more reliably. In indoor applications, such an approach cannot be adopted because of the presence of metallic objects, furniture, and building structures; these sources introduce the soft and hard-iron effects, which manipulate the geomagnetic field and make the measurements unreliable. Despite this issue, many solutions based on different ideas have been proposed in the literature to exploit magnetometers for localization and orientation purposes, such as the magnetic fingerprint approaches [20], or the use of magnetic information fused with other sensors (accelerometer, gyroscope, odometer) to help the system in the attitude estimation [21] [11] [14]. However, to reliably use the magnetic information in indoor and outdoor environments when a metallic object can affect the measurement, compensation for the disturbances is needed.

In the literature, there are some proposals for magnetic disturbances compensation. Authors in reference [22] deal with soft and hard-iron effects generated by metallic components or strong electrical currents in underwater vehicles where the space for mounting magnetic sensors is limited; they focused on the compensation for the static soft and hard-iron effects generated by the robot itself due to the structure and the permanent magnets of the motors, and the compensation for the dynamic hard-iron effects generated by strong current consumptions in cables near to the magnetometers. Static effects have been compensated using a calibration procedure,

whereas dynamic effects are filtered out by an algorithm that uses the information from multiple distributed small sensors installed on the vehicle; the filtering algorithm is based on the idea that in some cases distortions can affect only the flux density (strength component) and preserve the direction even if the disturbance is high, and vice versa, in some other cases distortions can affect only the direction and preserve the flux density. Based on these considerations, it is possible to estimate the probability of how a magnetometer in the array is disturbed; the flux density is modelled as a Gaussian distribution, whereas the three-dimensional direction component is modelled using the von Mises-Fisher distributions. The proposed approach compensates only for the disturbances produced by the robot itself, and it cannot deal with any external interference due to ferromagnetic objects.

In reference [23], authors deal with dynamic magnetic field distortions generated by the robot itself due to a change in the posture or a different current consumption. This type of problem arises in systems where it is not possible to install magnetometers far away from the sources of the distortion or in robots equipped with many moving parts (such as multiple legs or/and arms) that can change the configuration and modify the distribution of the soft and hard-iron effect sources. They propose a solution based on Machine Learning (ML) that is able to learn the model of the magnetic field distortions and provide the needed compensation. The idea is to use the ambient magnetic field to estimate the orientation or localization after compensation for the dynamic disturbances. The configuration of a robot can be inferred either using the proprioceptive sensor data or using an array of distributed magnetic sensors (as done in reference [22]). They adopt a multi-target function regression approach, proposing two solutions: the first one based on a Support Vector Regression (SVR) and the second one based on a Multi-Layer Perceptron (MLP) regression. The inputs of the function regression systems are the posture, the current consumptions of the motors, and the configuration of the robot; the outputs are the compensations of the magnetic field. The proposed system is able to deal with self-induced disturbances, but it cannot compensate for distortions induced by external metallic objects.

The authors in reference [6] adopt a magnetic fingerprint approach for the indoor localization of smartphones. The system uses Magnetic Field Magnitude (MFM) features that are generated by distortions of the geomagnetic field due to the presence of pillars, escalators, and large iron furniture. However, the magnetometer measurements are influenced by soft and hard-iron effects generated by the Printed Circuit Board (PCB) of the device itself. To deal with this problem and estimate the indoor magnetic field, authors derive the inverse model of the magnetometer measurement that enables compensation for the introduced errors. The proposed model considers additive and multiplicative interferences. The former includes the hard-iron effect and the sensor offset, whilst the latter includes the soft-iron effect, magnetometer nonorthogonality, and unequal gains. The proposed solution is able to compensate only for the disturbances introduced by the smartphone board itself,

and it cannot deal with soft and hard-iron effects introduced by further metallic objects that modify the magnetic features collected during the offline phase of the fingerprint approach.

In reference [24], the authors of the paper proposed a system for the neglect of disturbances induced by known metallic objects that are detected by a different technology, such as a stereo vision system or LiDAR; such technologies are able to identify the known objects and provide the distance and the angle between the object and the robot in the reference frame of the object itself. Then, an MLP neural network is used to estimate the disturbances generated by the known metallic object. The inputs of the Artificial Neural Network (ANN) are the distance and the angle, and the outputs are the three components to compensate for the disturbance of the known ferromagnetic object. The proposed concept considers only one type of ANN architecture and doesn't consider double hidden layer structure or other types of soft-computing tools that could be adopted to solve the problem.

Besides the aforementioned articles, the literature also proposes inference systems for localization purposes based on fuzzy techniques and magnetometers. In reference [25], the authors use the information from a three-axis gyroscope and a three-axis magnetometer that are provided as input to a combined Fuzzy Inference System (FIS) compensation and Kalman Filter (KF) system to estimate the relative and absolute orientation angles of the robot with high accuracy. Reference [26] proposes a system for an autonomous robot based on Adaptive Neuro FIS (ANFIS) that navigates in the north direction and it is able to avoid obstacles; the neuro system fuses the sensor information from a magnetic compass and a sonar; the former needs to determine the target angle and the latter needs to identify the obstacle. In reference [27], authors deal with the estimation of the orientation problem for Unmanned Aerial Vehicles (UAVs); their solution fuses the information from a three-axis gyroscope, a three-axis magnetometer, and a visual navigation system using a Complementary KF combined with fuzzy logic to adjust the gain of the filter to improve the robustness and accuracy of the system. In reference [28], the authors focus on a system for pedestrian localization by fusing information from the Global Positioning System (GPS), a digital compass consisting of a 3-axis semiconductor magnetometer and two tilt sensors, and an orientation tracker composed of a three-axis gyroscope, a three-axis accelerometer, and a three-axis magnetometer. The information from the digital compass and the orientation tracker is fused using a fuzzy system that provides an output that is fused with the GPS signal using an Extended KF (EKF). The rules of the fuzzy system determine how to combine the orientation data from the two sensors and decide whether to consider both or only one of them at a time. Authors in reference [29] deal with indoor smartphone localization adopting a magnetic fingerprint approach; they compensate for the soft and hard-iron effects introduced by the device itself and use a Fuzzy K-nearest neighbour classifier (described in [30]) to estimate the position. References [25] - [29] exploit magnetic information and also adopt the

fuzzy logic tool, but do not aim to deal with ferromagnetic disturbances compensation.

From a mathematical point of view, to solve the problem of disturbance compensation, different nonlinear modelling approaches can be adopted. In the literature, there are many proposals to deal with nonlinear modelling problems, and some valuable examples are the following. The authors in reference [31] proposed a system for the mobile robot pose estimation based on a specific algorithm that exploits the differences between the real sensor readings (from a laser scanner technology) and the virtual (or simulated) sensor readings obtained from a known map of the environment of work; the algorithm estimates the pose by looking for the best match between the two types of readings. In reference [32], a new concept for the parameters estimation of the nonlinear model of photovoltaic cells is proposed, and it is based on a Balancing Composite Motions Optimization (BCMO) technique that allows to model the system by minimizing the Root Mean Square Error (RMSE) between the experimental and simulated data. The authors in reference [33] proposed two nonlinear estimation approaches that are based on an EKF and a Takagi-Sugeno Fuzzy Observer, respectively; they deal with the control process of a Strip Winding System that is a nonlinear system characterized by a variable reference input, a variable moment of inertia with a constant increasing tendency, and variable parameters. Alternatively, the class of nonlinear modelling can also be addressed by adopting approaches based on multilayer neural networks as proposed in [34], in which the authors exploited an ANN to describe the relationship between the pollution rank and the geographic coordinates.

In agreement with all the aforementioned articles and to the best knowledge of the authors, the State-Of-the-Art (SOA) of the compensation for the soft and hard-iron effects can be summarized as reported in Table 1.

By observing Table 1, it is possible to note that the literature offers some different approaches for magnetic disturbances compensation but the proposed solutions in reference [22], [23], and [6] don't deal with the compensation for disturbances introduced by external ferromagnetic objects, and therefore those proposals can be effected by external soft and hard-iron effects. On the other hand, only reference [24] proposed an approach to compensate for magnetic disturbances induced by a known metallic object, but the authors considered only a solution with a single hidden layer ANN without considering other soft-computing tools that might improve performances.

This paper aims to estimate the magnetic disturbances induced by a known metallic object in systems for robot localization purposes. By adopting the main concept based on an ANN proposed in reference [24], new techniques based on different soft computing-based tools are proposed to estimate the magnetic disturbances for a known object. The paper exploits the capabilities of a double hidden layer ANN (which is the extension of the single layer ANN proposed in reference [24]), a FIS and the ANFIS approaches. The choice of these soft-computing tools is due to their flexibility and their capability to deal with nonlinear systems.

Table 1  
Summary of the SOA of the compensation for magnetic disturbances

Reference	Aim of the proposal	Drawback of the proposal
[22]	(i) To compensate for the static soft and hard-iron effects generated by the robot itself due to the structure and the permanent magnets of the motors. (ii) To compensate for the dynamic hard-iron effects generated by strong current consumptions in cables near to the magnetometers.	It cannot deal with any external disturbance induced by ferromagnetic objects.
[23]	To deal with dynamic magnetic field distortions generated by the robot itself due to a change in the posture or a different current consumption.	It cannot deal with any external disturbance induced by ferromagnetic objects.
[6]	To compensate for the disturbances (soft and hard-iron effects) induced by PCB.	It cannot deal with any external disturbance induced by ferromagnetic objects.
[24]	To compensate for the disturbances induced by known metallic objects	Only one type of soft computing tool was considered.

The main contributions of this article can be summarized as follows:

- Three novel approaches, respectively based on a double hidden layer ANN, a FIS and an ANFIS, are proposed to neglect disturbances induced by known metallic objects; they are based on the main concept proposed in reference [24].
- The obtained results by using the technique in reference [24] and all techniques here proposed are compared to each other evaluating their performances based on measured magnetic fingerprints of multiple objects.

The rest of the paper is organized as follows. Section 2 summarizes the exploited concept, and reports the used measurement data. Section 3 introduces the proposed techniques for the identification and compensation of magnetic disturbances. Section 4 reports all obtained results and provides a comparison among them. Finally, the conclusion summarizes the developed work and provides future work plans.

## 2 Exploited Concepts and used Measurement Data

The proposed techniques in this article aim to provide the value of the three magnetic disturbance components induced by a known metallic object in order to compensate for the magnetometer measurements. The techniques exploit the concept proposed in reference [24] and adopt the same basic assumptions. More

precisely, it is supposed to have a robot equipped with a technology (e.g., stereo vision system, LiDAR, etc.) that can detect the known metallic object and provide the distance  $d$  and angle  $\alpha$  in the reference frame of the object; the two variables are given as inputs to a soft-computing technique that gives as outputs the three components of the disturbance. The concept is summarized in Figure 1 [24], where it is possible to see (i) the schematic of the robot with a magnetometer sensor  $S$  and the object (in red), and (ii) the input and output variables diagram for a generic soft-computing technique.

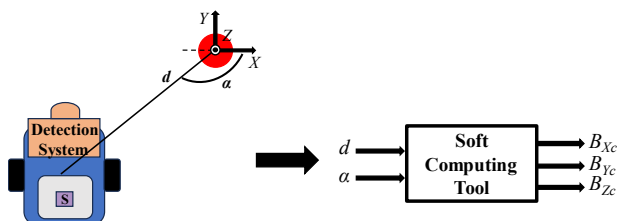


Figure 1

On the left, the scheme of the robot and the detected known object (in red) with its reference frame; on the right, the soft computing tool with its input and output variables [24]. The three outputs are the three components of the vector  $\mathbf{B}_c$ .

In order to obtain the compensated measurement vector  $\mathbf{B}$ , the generated outputs  $\mathbf{B}_c$  provided by the soft-computing techniques need to be subtracted from the magnetometer outputs  $\mathbf{B}_m$ , and it is given by the following vectorial equation:

$$\mathbf{B} = \mathbf{B}_m - \mathbf{B}_c. \quad (1)$$

Furthermore, it is supposed that the magnetic fingerprint (or disturbances) of a given metallic object is known, is time-invariant, and can be calculated by adopting the technique proposed in reference [35]. By adopting such an approach, in each point of the space around an object the disturbances are obtained by subtracting the magnetic field measured during the undisturbed scenario from the magnetic field measured during the disturbed one, and it is given as:

$$\mathbf{B}_{fp} = \mathbf{B}_{ds} - \mathbf{B}_{us} \quad (2)$$

where  $\mathbf{B}_{fp}$  is the magnetic field vector of the fingerprint,  $\mathbf{B}_{ds}$  is the magnetic field vector of the disturbed scenario, and  $\mathbf{B}_{us}$  is the magnetic field vector in the undisturbed scenario.

As done in reference [24], three metallic objects were investigated: (i) a fluxmeter, (ii) a C-shape structure, and (iii) a complex object composed of two C-shape structures. For each of them, the magnetic fingerprint was measured using the HMC5883L three-axis magnetometer digital sensor that was installed as an End Effector on the ABB IRB 140 industrial robotic arm; the three axes of the sensor frame are parallel to the three axes object frame. In Figure 2, the used measurement setup to obtain the magnetic disturbances and the investigated objects are shown.

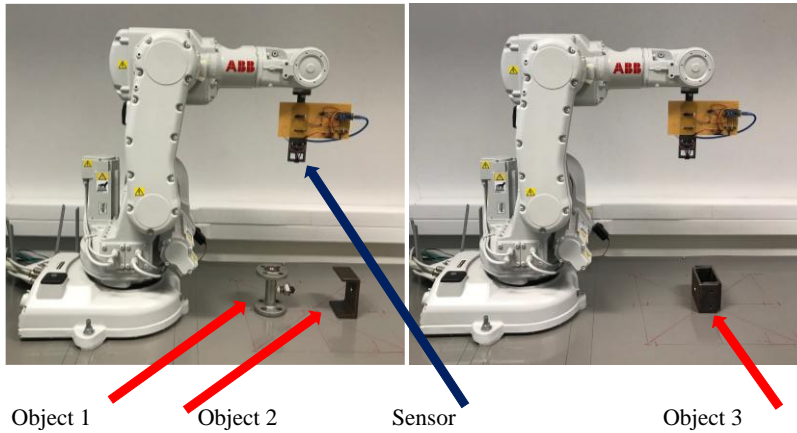


Figure 2

Measurement setup for the magnetic disturbances with investigated objects

For each object, an area of  $40 \times 40$  cm was considered where in the middle the object under investigation was placed. Samples were collected along 41 straight trajectories, in points spaced 1 cm from each other generating a grid. To avoid collision between the end effector and the object, some samples were not recorded in a limited square area around the object itself. The applied sampling rate was 50 Hz and, in each considered point of the grid, 100 samples were recorded and averaged to reduce the effect of noise. For example, the 2-dimensional heat maps of the three components of object 2 are reported in Figure 3. The white square areas in the middle of the pictures represent the space where measurements were not recorded due to the presence of the object itself.

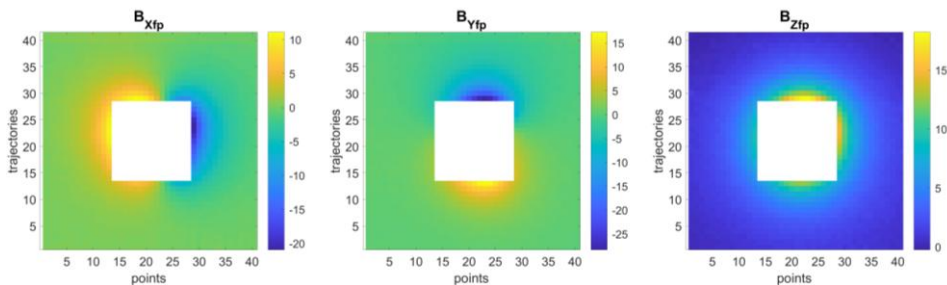


Figure 3

The heat maps of the fingerprint of the object 2. The color bar values are  $\mu\text{T}$

In order to provide a better comprehension of the entire method related to the technique proposed in reference [24] and the techniques here proposed, Table 2 summarizes all steps, providing a complete view of the whole procedure.

Table 2  
Summary of the procedure

Step	Schematic representation	Description
1	<p>Robotic Arm, Sensor, Investigated Object, Bench, View from the top, Each dot is a point of the grid</p>	<p>Measurements of the magnetic field with and without the presence of the investigated object.</p>
2	<p><math>B_{x_{fp}}</math>, <math>B_{y_{fp}}</math>, <math>B_{z_{fp}}</math>, Inhomogeneities, points</p>	<p>Extraction of the object disturbance (or fingerprint) by applying equation 2.</p>
3	<p><math>B_{fp}</math>, <math>d</math>, <math>\alpha</math>, Soft Computing Tool, <math>B_{xc}</math>, <math>B_{yc}</math>, <math>B_{zc}</math></p>	<p>Designing and training of a soft compute technique by using the obtained fingerprint at Step 2.</p>
4	<p><math>d</math>, <math>\alpha</math>, Soft Computing Tool, <math>B_{xc}</math>, <math>B_{yc}</math>, <math>B_{zc}</math></p>	<p>Offline test of the designed technique. Direct comparison between <math>B_{fp}</math> and <math>B_c</math>, and estimation of the errors. The <math>d</math> and <math>\alpha</math> variables are in relation to the position of each point of the grid.</p>
5	<p>Detection System, <math>d</math>, <math>\alpha</math>, Soft Computing Tool, <math>B_{xc}</math>, <math>B_{yc}</math>, <math>B_{zc}</math></p>	<p>Online test in which the variables <math>d</math> and <math>\alpha</math> are provided by the detection system.</p>

### 3 Proposed Compensation Techniques and Tested Algorithms

Differently from the proposed technique in [24], in which an MLP ANN with only one hidden layer was adopted as a soft-computing technique, in this paper, the original concept was modified by using different soft computing tools and proposing three new techniques that exploit an MLP with two hidden layers, the FIS, and the ANFIS. The authors made the implementations publicly available in the Supplementary Online Material [36] in order to help other lab teams in the development of similar algorithms. The algorithms are presented as follows.

#### 3.1 Artificial Neural Network

By considering the block diagram in Figure 1, an MLP ANN architecture composed of an input layer, two hidden layers (with the same number of neurons), and an output layer, is adopted. Each neuron in each layer is fully connected with each neuron in the next one. Both the distance and angle of the identified object are given as inputs at the first layer. As for the two hidden layers, the used activation functions are sigmoids and different numbers of neurons between 1 and 100 were tested to find the optimal setup. The final layer provides the outputs, which are the three components of the estimated disturbance; the linear activation function is applied in this layer. The training process is conducted using the Levenberg–Marquardt backpropagation and providing as target data the  $\mathbf{B}_{fp}$  values of the fingerprint. To evaluate the performances of each trained architecture, the Mean Squared Error (MSE) is used, and, as done in reference [24], the training data are obtained considering 70% of the grid points and using the other 30% for the validation process. Such a training/testing ratio of 70/30 is an empirical data splitting value that is largely accepted in literature to avoid overfitting [37]. In Figure 4, the adopted architecture is shown. In addition, it is specified that such an architecture choice is based on the author’s experience and on the work developed in reference [24].

#### 3.2 Fuzzy Inference System

The original idea to use an ANN is modified, and the MLP is substituted with three Mamdani FISs (one for each component of the magnetic field).

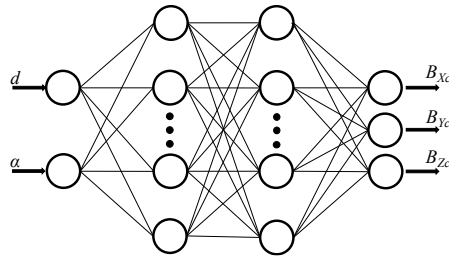


Figure 4

The architecture of the two hidden layers ANN

Distance and angle inputs are given to a function  $F(d, \alpha)$  that provides as outputs the coordinate  $(x, y)$  of the object in the object reference frame. Then, the position coordinates are given as inputs to the FISs which provide as output the three magnetic components of the compensation values, i.e.,  $B_{Xc}$ ,  $B_{Yc}$ ,  $B_{Zc}$ . The function  $F(d, \alpha)$  is given as:

$$F(d, \alpha) = \begin{cases} x = d \cdot \cos(\alpha) \\ y = d \cdot \sin(\alpha) \end{cases} \quad (3)$$

The architecture of the FIS technique is reported in Figure 5, whilst in Figure 6 an example of one of the three FIS structures used in the technique is shown for the component  $B_{Xc}$ .

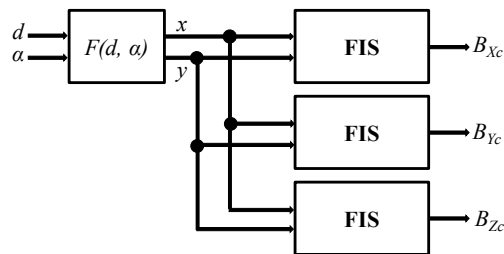


Figure 5

The overall architecture of the FIS technique

For each component of the magnetic field, the FIS is designed with 11 Membership Functions (MFs) per input because, considering the investigated area around the object, i.e., a squared area with 41 trajectories and 41 points per each trajectory, the coordinates at every 4 cm both along  $x$  and  $y$  were chosen as reference coordinates; this choice gives rise to 11 MFs per each input. It is highlighted that the higher the number of MFs, the higher the resolution, and a such high number of MFs was due to obtaining results comparable with the other investigated techniques.

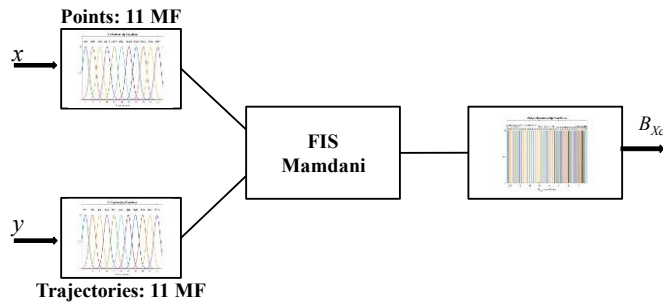


Figure 6

The structure of the FIS only for the component  $B_{xc}$

Furthermore, the chosen MFs are Gaussian, and they have as average one of the reference coordinates (either along  $x$  or  $y$ ), and as variance a value of  $1.75 \text{ cm}^2$  that was obtained by empirical trials. Different types of MFs, such as triangular or trapezoidal, were also tested, but they provided worse results than the Gaussian function, which gives the lowest maximum absolute error using the chosen variance. The input MFs for the  $x$  and  $y$  coordinates are set in the same manner, and, as an example, the  $x$  input MFs are reported in Figure 7.

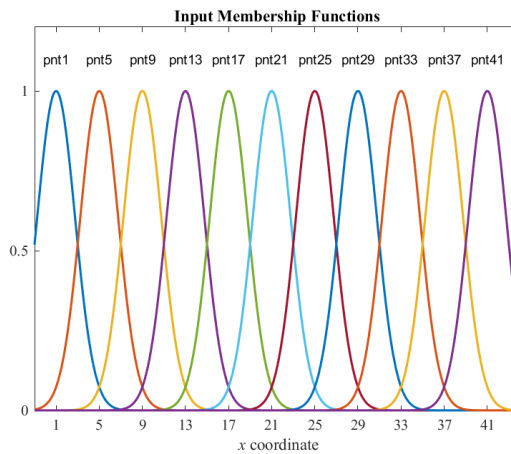


Figure 7

The 11 input MFs for the component  $x$

The output MFs are obtained by discretizing the magnetic field range of the disturbance, i.e., the  $B_{fp}$  values of the fingerprint, with steps of  $1 \mu\text{T}$  between the minimum and the maximum of each component and for each investigated object. The used function is trapezoidal with the minor base of  $0.4 \mu\text{T}$  and the major base of  $0.42 \mu\text{T}$  that were obtained by empirical trials. Also, different types of functions, such as triangular and Gaussian, were tested, but the trapezoidal one provided the best performance. Furthermore, a high number of MFs was needed to obtain performances that are comparable with the other techniques. Because each object and each component are different, many sets of output MFs are developed, and as an example, the output MFs for the component  $B_{Xc}$  of the object number 2 is reported in Figure 8.

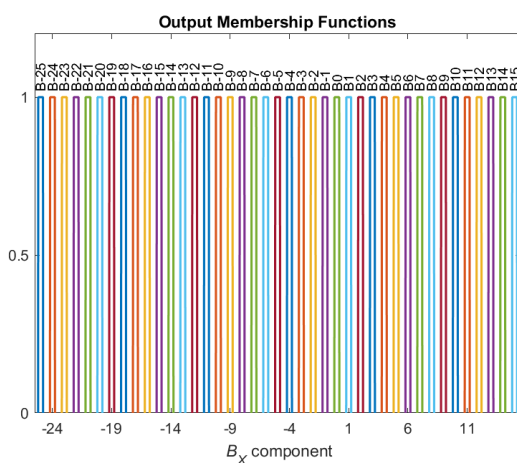


Figure 8

The output MFs for the component  $B_{Xc}$

The used designing software is the Fuzzy Logic Designer tool of MATLAB. For each FIS, a total of 112 rules generated using each trajectory and each considered point of the area under investigation were entered, and they are given as:

$$\text{If (Point is } pnt1) \text{ AND (Trajectory is } trj1), \text{ then } (B_X \text{ is } B0) \quad (4)$$

where  $pnt1$  and  $trj1$  are respectively the  $x$  and  $y$  reference input coordinates,  $B_X$  is the variable of the output, and  $B0$  is the selected value for the entered reference coordinate. It is noted that the number of total rules is not equal to 121 (obtained by multiplying the number of the MFs:  $11 \times 11$ ) as it could be expected because in the space occupied by the object, it is not possible to measure the magnetic disturbances. Finally, the obtained FIS surface of the component  $B_{Xc}$  of the object number 2 is reported in Figure 9 as an example.

### 3.3 Adaptive Neuro Fuzzy Inference System

In this technique, the FIS blocks described in the previous paragraph are substituted with ANFIS blocks holding the same overall architecture as shown in both Figure 5 and Figure 6. For each component of the magnetic field and each investigated object, two types of techniques were designed: the first one with 11 MFs for each input (referred to as ANFIS 11), and the second one with 41 MF (referred to as ANFIS 41).

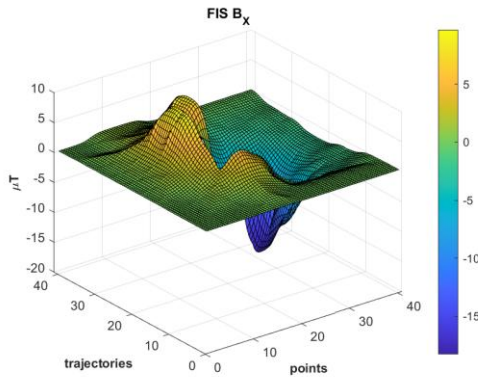


Figure 9  
The FIS surface of the component  $B_{xc}$  (object 2)

Both of them are designed with the Neuro-Fuzzy Designer Toolbox of MATLAB. As ANFIS 11, the train data for each component and each object are generated by the magnetic fingerprint of the object itself by extracting the value of the disturbance by considering points spaced of 4 cm along each axis as done for the FIS technique. Then, the neuro system is set with 11 triangular MFs for each input and a constant

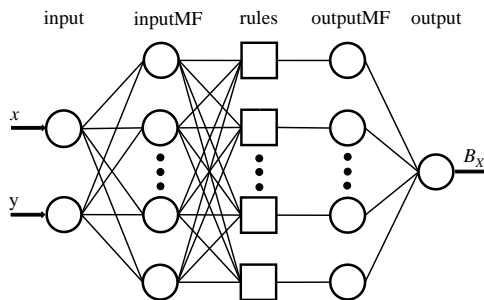


Figure 10  
The architecture of ANFIS with a generic number of MF for the component  $B_{xc}$

MF as output; the set optimization technique is hybrid with 1000 training epochs, and the convergence is reached after about 650 epochs with a relative training error in the order of a few  $10^{-6}$   $\mu\text{T}$  for each component and each object. As ANFIS 41, the same steps are adopted, but with the difference that each of the 41 trajectories and each of the 41 points in each trajectory are considered and used as training data. The neuro system is set with 41 triangular MFs for each input and a constant MF as output; the set optimization technique is hybrid with 100 training epochs; the convergence is reached after a few epochs with a relative training error in the order of a few  $10^{-6}$   $\mu\text{T}$  for each component and each object. As example, in Figure 10, the structure of the used ANFIS for both the 11 and 41 techniques is reported for the  $B_x$  component.

## 4 Tests

For each considered object, the error between the measured value of the disturbance and the estimated one by adopting one of the proposed techniques is given as:

$$e_I(x, y) = B_{I_{fp}}(x, y) - B_{Ic}(x, y) \quad (5)$$

where, for the considered object,  $I$  identifies one of the three components of the magnetic field,  $e_I$  is the error of the  $I$ -th magnetic component,  $x$  and  $y$  are the coordinates of the tested points, and  $B_{I_{fp}}(x, y)$  and  $B_{Ic}(x, y)$  are the  $I$ -th magnetic field component of the measurement and the provided compensation, respectively.

The used evaluation parameters to evaluate the performance of each technique are the Mean Absolute Error (MAE) of each component and the total MAE. The former is computed using the following equations:

$$e_{MAE_I}(x, y) = \frac{1}{N} (\sum_x \sum_y |B_{I_{fp}}(x, y) - B_{Ic}(x, y)|) \quad (6)$$

where  $N$  is the total number of measured points in the area. The latter is given as:

$$e_{MAE_t}(x, y) = \frac{1}{3N} (\sum_x \sum_y (\sum_I |B_{I_{fp}}(x, y) - B_{Ic}(x, y)|)) \quad (7)$$

The obtained MAEs of each proposed new technique, the original single hidden layer ANN in reference [24], and the case without any compensation were investigated to compare the performances. It is outlined that the proposed concepts have been tested offline because no real robot localization system has been implemented. In other words, the proposed concepts were tested by providing the distance and angle as inputs; then, the provided outputs of each technique were compared with the value obtained by measuring the fingerprint of the known metallic object. These tests aim to validate the theoretical feasibility of the concepts.

As for the double hidden layer ANN technique, the trend of the total MAE as a function of the number of neurons is reported in Figure 11. The graph shows that

the convergence is reached very soon for the second and third objects (about after 15 neurons), whereas the first one has a more complex trend with some sudden high spikes before the stabilization that is reached at 40 neurons. After convergence, the first and the second objects show an irregular trend after 51 neurons where some little spikes are present until the end of the investigated neurons. The strange behaviour is more marked for the first object which had a stranger trend also in the

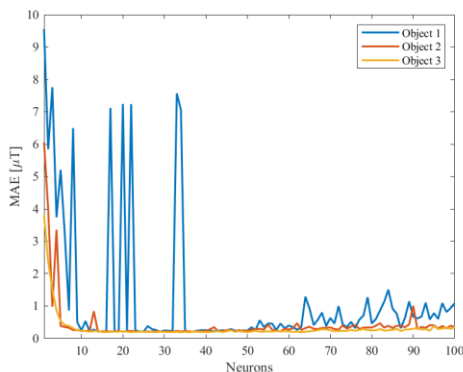


Figure 11

The MAE as a function of neurons for the ANN architecture with two hidden layers

Table 3

Number of neurons for each tested ANN architecture and for each tested object

Object	1 Hidden Layer [24]	2 Hidden Layer
1	79	36
2	93	24
3	69	36

results obtained in reference [24] for a single hidden layer. However, to compare the performances among other techniques here proposed, the number of neurons that provides the lowest total MAE for each architecture and each object has been chosen, and their values are summarized in Table 3, where the numbers for the single hidden layer are reported as well. In other words, for each object, only the architecture (with a specific number of neurons) that provides the best results is considered.

In general, by considering the data in Table 3 and the results in Figure 11, it is possible to note that the ANN convergence depends on the considered object and the number of considered hidden layers.

Error trends are calculated using equation (5), and, as an example of the obtained outputs, the trends of the X component of object 2 for each technique are reported in Figure 12-16. The square area inside the graph at the centre where the error is

zero is the space where the measurements were not collected. Some considerations that are in common with all results for each object are the following. In all graphs, it is possible to observe an irregular trend of the error with some limited spikes. The two MLPs show very similar behaviours, even though the double hidden layer

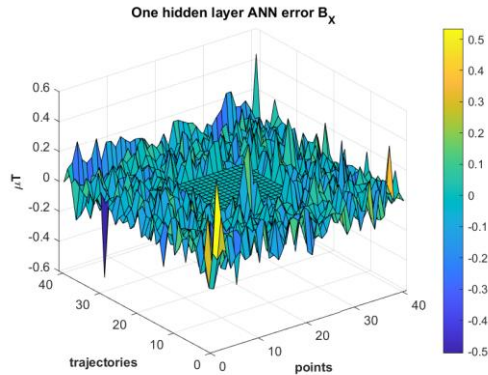


Figure 12

The error of component  $B_x$ . (object 2) for the ANN technique with one hidden layer

ANN has several spikes less than the single one. FIS shows a very coarse trend, but

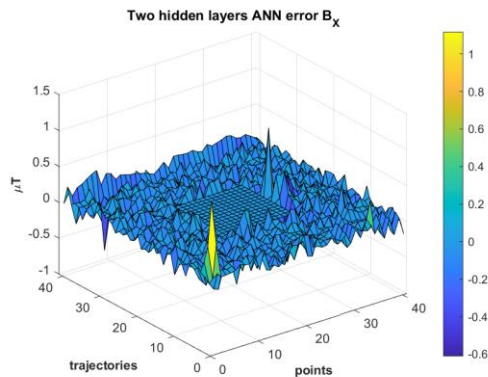


Figure 13

The error of component  $B_x$ . (object 2) for the ANN technique with two hidden layers

it is expected because the number of MFs is limited. A little bit better for ANFIS 11, but the limitation in the MFs gives rise to a trend that is very similar to FIS. As ANFIS 41, the scale of the error is three orders less than the others and it shows to be the most accurate whatever the considered object.

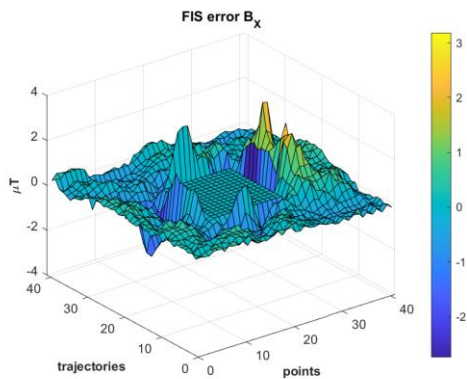


Figure 14  
The error of component  $B_x$ . (object 2) for the FIS technique

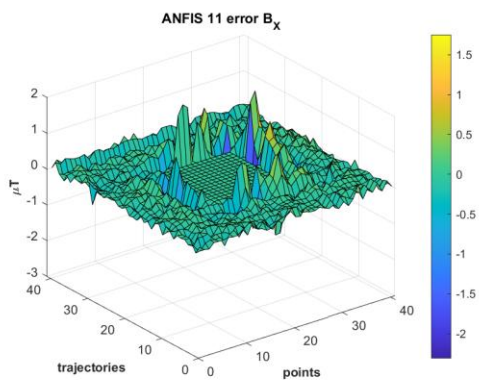


Figure 15  
The error of component  $B_x$ . (object 2) for the ANFIS 11 technique

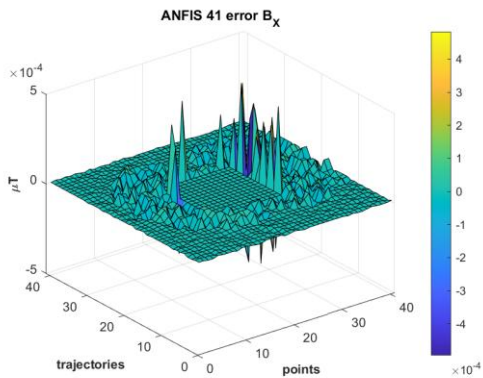


Figure 16  
The error of component  $B_x$ . (object 2) for the ANFIS 41 technique

For instance, as for object 2, Figures 17-18 report the component  $B_X$  of the disturbance that is, respectively, obtained by measurements and by adopting ANFIS 41. The latter is obtained by providing inputs every 0.5 cm that is less than the measurement resolution.

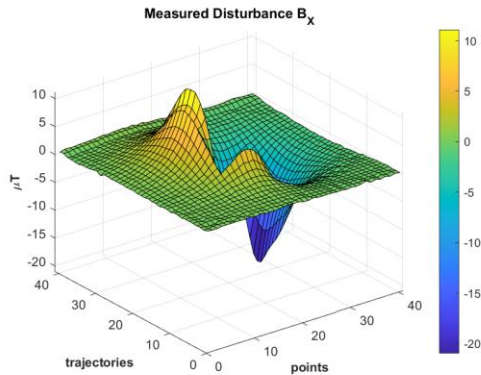


Figure 17

The measured fingerprint component  $B_{Xfp}$ . (object 2)

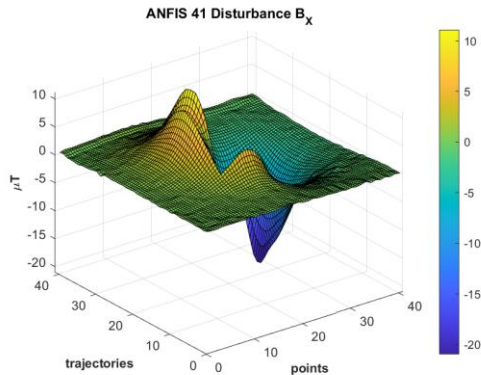


Figure 18

The generated fingerprint component  $B_{Xc}$ . (object 2), by adopting ANFIS 41

All obtained maximum errors and MAEs of the original technique, of each new proposed technique, and the case without any compensation are reported in Table 4-5 as a summary of the obtained results.

Table 4  
The maximum errors for all techniques and Objects

All values in $\mu\text{T}$						
X axis						
Object	Before compensation	After ANN compensation 1 hidden layer [24]	After ANN compensation 2 hidden layer	After FIS (11 MF per Input) compensation	After ANFIS (11 MF per Input) compensation	After ANFIS (41 MF per Input) compensation
1	68.21	1.6664	1.5438	33.956	9.9701	$5.3169 \cdot 10^{-4}$
2	20.96	0.5341	1.1189	3.1833	2.3106	$4.953810^{-4}$
3	14.281	0.3137	0.78114	2.5640	1.3644	$4.875910^{-4}$
Y axis						
Object	Before compensation	After ANN compensation 1 hidden layer [24]	After ANN compensation 2 hidden layer	After FIS (11 MF per Input) compensation	After ANFIS (11 MF per Input) compensation	After ANFIS (41 MF per Input) compensation
1	52.294	2.4561	3.8310	50.682	28.203	$5.2552 \cdot 10^{-4}$
2	28.319	0.5153	0.55703	5.4384	3.7215	$4.8956 \cdot 10^{-4}$
3	13.713	0.6207	1.1460	2.1824	1.5905	$5.1029 \cdot 10^{-4}$
Z axis						
Object	Before compensation	After ANN compensation 1 hidden layer [24]	After ANN compensation 2 hidden layer	After FIS (11 MF per Input) compensation	After ANFIS (11 MF per Input) compensation	After ANFIS (41 MF per Input) compensation
1	110.18	1.5427	2.1531	35.258	18.114	$2.3258 \cdot 10^{-3}$
2	18.222	0.7617	0.88379	3.2117	1.7802	$5.1140 \cdot 10^{-4}$
3	9.5048	0.4085	1.2136	2.4436	1.7178	$5.8919 \cdot 10^{-5}$

The data are divided into the errors related to each object and each component. By evaluating the tables, it is possible to infer that performance depends also on the investigated object besides the considered technique. Very meaningful is the case of object 1, where FIS provides, as the worst case, a maximum error of  $50.682 \mu\text{T}$  for the  $B_Y$  component that is slightly improved by using ANFIS 11 which provides  $28.2031 \mu\text{T}$ ; they are of the same order of magnitude as the case without any compensation and, therefore, cannot be considered acceptable. Altogether, object 1 is the hardest to compensate for the disturbance for all techniques, and acceptable maximum errors are provided only by ANNs and ANFIS 41 techniques, which provide the worst maximum errors of  $3.8310 \mu\text{T}$  and  $2.3258 \cdot 10^{-3} \mu\text{T}$ , respectively. As for the MAE of object 1, FIS is not able to significantly compensate for the disturbance because it gives errors in the order of a few  $\mu\text{T}$  which are comparable to the case without any compensation; on the contrary, FIS 11 works better, giving

in the worst case an MAE of about  $0.4 \mu\text{T}$ . The remaining other techniques, i.e., ANNs and ANFIS 41, provide more satisfying results in the order of  $0.07 \mu\text{T}$  and  $10^{-5} \mu\text{T}$ , respectively.

In general, better results are obtained by considering objects 2 and 3; in these cases,

Table 5  
The MAEs for all techniques and Objects

All values in $\mu\text{T}$						
X axis						
Object	Before compensation	After ANN compensation 1 hidden layer [24]	After ANN compensation 2 hidden layer	After FIS (11 MF per Input) compensation	After ANFIS (11 MF per Input) compensation	After ANFIS (41 MF per Input) compensation
1	2.9675	0.0693	0.06918	3.64480	0.29804	$2.9010 \cdot 10^{-5}$
2	1.9709	0.07149	0.07425	0.37928	0.15944	$2.0413 \cdot 10^{-5}$
3	1.7898	0.06474	0.06266	0.32054	0.12000	$1.9315 \cdot 10^{-5}$
Y axis						
Object	Before compensation	After ANN compensation 1 hidden layer [24]	After ANN compensation 2 hidden layer	After FIS (11 MF per Input) compensation	After ANFIS (11 MF per Input) compensation	After ANFIS (41 MF per Input) compensation
1	3.0884	0.07626	0.07673	1.80450	0.39692	$3.0946 \cdot 10^{-5}$
2	2.0475	0.07446	0.07557	0.38560	0.18605	$1.9893 \cdot 10^{-5}$
3	1.9242	0.07235	0.06682	0.32655	0.13174	$2.0057 \cdot 10^{-5}$
Z axis						
Object	Before compensation	After ANN compensation 1 hidden layer [24]	After ANN compensation 2 hidden layer	After FIS (11 MF per Input) compensation	After ANFIS (11 MF per Input) compensation	After ANFIS (41 MF per Input) compensation
1	2.8802	0.07521	0.07418	1.73240	0.45068	$2.9784 \cdot 10^{-5}$
2	2.9077	0.07232	0.07351	0.33637	0.16825	$2.7286 \cdot 10^{-5}$
3	0.8742	0.06942	0.07212	0.39290	0.18834	$6.5660 \cdot 10^{-6}$
Overall						
Object	Before compensation	After ANN compensation 1 hidden layer [24]	After ANN compensation 2 hidden layer	After FIS (11 MF per Input) compensation	After ANFIS (11 MF per Input) compensation	After ANFIS (41 MF per Input) compensation
1	2.9787	0.07359	0.07336	2.3939	0.38186	$2.9913 \cdot 10^{-5}$
2	2.3087	0.07275	0.07444	0.36710	0.17124	$2.2530 \cdot 10^{-5}$
3	1.5294	0.06883	0.06720	0.34666	0.146693	$1.5312 \cdot 10^{-5}$

the two ANNs provide similar performance with an acceptable maximum error in the range between  $0.3 \mu\text{T}$  and  $1.2 \mu\text{T}$  and an acceptable MAE in the order of  $0.07$

$\mu\text{T}$ . FIS and ANFIS 11 provide comparable results, with maximum errors in the range between  $1.3 \mu\text{T}$  and  $5.4 \mu\text{T}$ , and MAE errors in the range between  $0.12 \mu\text{T}$  and  $0.39 \mu\text{T}$ . Finally, ANIFS 41 provides the best results with a maximum error in the order of  $10^{-4} \mu\text{T}$  and MAEs in the order of  $10^{-5} \mu\text{T}$ .

In summary, by considering both maximum errors and MAEs, FIS is the one that provided the worst performance (not always acceptable) despite the high number of adopted MFs; a little bit better results were provided by ANFIS 11, but they still are not always satisfactory. The two ANNs provide similar results for all objects with acceptable values that are comparable to each other. They are in the order of a few  $\mu\text{T}$  and cents  $\mu\text{T}$  for the maximum error and the MAE, respectively.

In the end, ANFIS 41 provides the best performance, providing good compensation for the disturbances and with errors that are at least three orders of magnitude smaller than the other ones in all cases.

## Conclusion

In this paper, four novel techniques for disturbance compensation have been proposed. They are a modified version of the technique proposed in reference [24], where the original single hidden layer ANN is substituted in each technique, respectively, with the double hidden layer ANN, the FIS, the ANFIS 11, and the ANFIS 41. Each of them was tested by computing the maximum errors and MAEs. The FIS technique is the one that provides the worst performance, particularly for object 1, with outputs not always acceptable; similar results a little bit improved are obtained with ANFIS 11, but still with poor performance for object 1. The single-layer and the double-layer ANNs have similar performances for all of the tested objects that can be considered altogether acceptable. As for ANFIS 41, it performs much better than other techniques, providing error values with a difference of at least three orders of magnitude less. Of all the proposed techniques, only the two MLP ANNs and ANFIS 41 can be considered suitable for further study by testing them in a real-time robotic localization system. In addition, it is specified that in this work, the presented new techniques were tested offline because no real localization systems have been implemented. However, the results suggest that the main concept proposed in [24] and here further developed offers a theoretical way to compensate for external magnetic disturbance induced by a known metallic object.

Finally, all the techniques here proposed and considered have the issue that the magnetic fingerprint of the identified object must be already known in advance, and it is a drawback; for this, future goals are to develop more generic techniques to compensate for unknown objects.

## Acknowledgement

The work was supported by the National Research, Development, and Innovation Fund of Hungary through project no. 142790 under the FK\_22 funding scheme.

## References

- [1] B. Lv, Y. Qin, H. Dai, and S. Su: Improving localization success rate of three magnetic targets using individual memory-based WO-LM algorithm, *IEEE Sensors Journal*, 2021, Vol. 21, No. 19, pp. 21750-21758
- [2] M. Yousefi, H. N. Pishkenari, and A. Alasty: A fast and robust magnetic localization technique based on elimination of the orientation variables from the optimization, *IEEE Sensors Journal*, 2021, Vol. 21, No. 19, pp. 21885-21892
- [3] Y. Wang, Q. Fu, and Y. Sui: A Robust Tracking Method for Multiple Moving Targets Based on Equivalent Magnetic Force, *Micromachines*, 2022, Vol. 13, No. 11, pp. 2018
- [4] B. R. Page, R. Lambert, N. Mahmoudian, D. H. Newby, E. L. Foley, T. W. Kornack: Compact Quantum Magnetometer System on an Agile Underwater Glider. *Sensors* 2021, Vol. 21, No. 4, pp. 1092
- [5] A. Solin, S. Sarkka, J. Kannala, and E. Rahtu: Terrain navigation in the magnetic landscape: Particle filtering for indoor positioning, *European Navigation Conference (ENC 2016)*, 2016, pp. 1-9
- [6] W. Shao, F. Zhao, C. Wang, H. Luo, T. Muhammad Zahid, Q. Wang, and D. Li: Location Fingerprint Extraction for Magnetic Field Magnitude Based Indoor Positioning, *Journal of Sensors*, 2016, Vol. 2016, pp. 1945695
- [7] M. Štancel, J. Hurtuk, M. Hulič, and J. Červeňák: Indoor atlas service as a tool for building an interior navigation system. *Acta Polytechnica Hungarica*, 2021, Vol. 18, pp. 87-110
- [8] R. Hostettler and P. M. Djurić: Vehicle Tracking Based on Fusion of Magnetometer and Accelerometer Sensor Measurements With Particle Filtering, *IEEE Transactions on Vehicular Technology*, Nov. 2015, Vol. 64, No. 11, pp. 4917-4928
- [9] N. Wahlström and F. Gustafsson: Magnetometer Modeling and Validation for Tracking Metallic Targets, *IEEE Transactions on Signal Processing*, Feb. 01 2014, Vol. 62, No. 3, pp. 545-556
- [10] J. Jung, S. -M. Lee and H. Myung: Indoor Mobile Robot Localization and Mapping Based on Ambient Magnetic Fields and Aiding Radio Sources, *IEEE Transactions on Instrumentation and Measurement*, July 2015, Vol. 64, No. 7, pp. 1922-1934
- [11] P. Sarcevic, D. Csik, and A. Odry: Indoor 2D Positioning Method for Mobile Robots Based on the Fusion of RSSI and Magnetometer Fingerprints, *Sensors*, 2023, Vol. 23, No. 4, pp. 1855
- [12] W. Lv, Y. Kang, and J. Qin: Indoor localization for skid-steering mobile robot by fusing encoder, gyroscope, and magnetometer, *IEEE Transactions*

- on Systems, Man, and Cybernetics: Systems; 2017, Vol. 49, No. 6, pp. 1241-1253
- [13] L. Fan, C. Kang, X. Zhang, Q. Zheng, and M. Wang: An efficient method for tracking a magnetic target using scalar magnetometer array, SpringerPlus, 2016, Vol. 5, No. 1, p. 502
- [14] A. Odry, I. Kecskes, D. Csik, H. A. Hashim, and P. Sarcevic: Adaptive Gradient-Descent Extended Kalman Filter for Pose Estimation of Mobile Robots with Sparse Reference Signals, In 2022 IEEE/RSJ International Conference on Intelligent Robots and Systems (IROS), October 2022, pp. 4010-4017
- [15] T. Mac Thi, C. Copot, and R. A. Cajo Diaz: Towards an autonomous landing system in presence of uncertain obstacles in indoor environments, Acta Polytechnica Hungarica, 2021, Vol. 18, No. 3, pp. 197-220
- [16] J. Callmer, M. Skoglund, and F. Gustafsson: Silent localization of underwater sensors using magnetometers, Eurasip Journal on Advances in signal processing, 2010, pp. 1-8
- [17] A. Poulouse, J. Kim, and D. S. Han: A sensor fusion framework for indoor localization using smartphone sensors and Wi-Fi RSSI measurements, Applied Sciences, 2010, Vol. 9, No. 20, p. 4379
- [18] P. Sarcevic, D. Csík, R. Pesti, M. Stefanoni, J. Sárosi, and Á. Odry: Fingerprint-based fusion of magnetic field data with multiple wireless technologies for indoor mobile robot positioning, 2023 13<sup>th</sup> International Conference on Indoor Positioning and Indoor Navigation (IPIN), Nuremberg, Germany, 2023, pp. 1-6
- [19] S. Moafipoor, D. A. Grejner-Brzezinska, and C. K. Toth: Adaptive calibration of a magnetometer compass for a personal navigation system, In IGNSS Symposium, December 2007
- [20] G. Ouyang, and K. Abed-Meraim: A Survey of Magnetic-Field-Based Indoor Localization, Electronics, 2022, Vol. 11, No. 6, p. 864
- [21] B. Kim and S. H. Kong: A novel indoor positioning technique using magnetic fingerprint difference, IEEE Transactions on Instrumentation and Measurement, 2016, Vol. 65, No. 9, pp. 2035-2045
- [22] L. Christensen, C. Gaudig and F. Kirchner: Distortion-robust distributed magnetometer for underwater pose estimation in confined UUVs, OCEANS 2015 - MTS/IEEE Washington, 2015, Washington, DC, USA, pp. 1-8
- [23] L. Christensen, M. Krell and F. Kirchner: Learning magnetic field distortion compensation for robotic systems, 2017 IEEE/RSJ International Conference on Intelligent Robots and Systems (IROS), September 2017, pp. 3516-3521
- [24] M. Stefanoni, Á Odry, and P. Sarcevic: A Neural Network-Based Approach for the Identification and Compensation of Magnetic Disturbances in Mobile

- Robot Localization, In 2023 IEEE 17<sup>th</sup> International Symposium on Applied Computational Intelligence and Informatics (SACI), May 2023, pp. 000393-000398
- [25] H. - Y. Chung, C. - C. Hou and Y. - S. Chen: Indoor Intelligent Mobile Robot Localization Using Fuzzy Compensation and Kalman Filter to Fuse the Data of Gyroscope and Magnetometer, in IEEE Transactions on Industrial Electronics, Vol. 62, No. 10, pp. 6436-6447
- [26] S. U. Deshpande and S. S. Bhosale: Adaptive neuro-fuzzy inference system based robotic navigation, In 2013 IEEE International Conference on Computational Intelligence and Computing Research, December 2013, pp. 1-4
- [27] Q. Yang and L. Sun: A fuzzy complementary Kalman filter based on visual and IMU data for UAV landing, Optik, 2018, Vol. 173, pp. 279-291
- [28] E. P. Herrera, R. Quiros, G. Fabregat, M. Ribo and A. Pinz: Pedestrian localization system based on Kalman filter and fuzzy logic, In SENSORS, 2006 IEEE, 2006, pp. 1183-1186
- [29] G. Ouyang and K. Abed-Meraim: Analysis of Magnetic Field Measurements for Mobile Localisation, In 2021 International Conference on Indoor Positioning and Indoor Navigation (IPIN) IEEE, November 2021, pp. 1-8
- [30] J. M. Keller, M. R. Gray and J. A. Givens: A fuzzy k-nearest neighbor algorithm, IEEE Transactions on systems, man, and cybernetics; 1985, Vol. 4, pp. 580-585
- [31] C. Pozna, R. E. Precup and P. Földesi: A novel pose estimation algorithm for robotic navigation, Robotics and Autonomous Systems; 2015, Vol. 63, pp. 10-21
- [32] N. N. Son and L. T. Vinh: Parameter estimation of photovoltaic model, using balancing composite motion optimization, Acta Polytechnica Hungarica; 2022, Vol. 19, No. 11, pp. 27-46
- [33] A. I. Szedlak-Stinean, R. E. Precup, E. M. Petriu, R. C. Roman, E. L. Hedrea, and C. A. Bojan-Dragos: Extended Kalman filter and Takagi-Sugeno fuzzy observer for a strip winding system. Expert Systems with Applications; 2022, Vol. 208, No. 118215
- [34] G. Duka and S. Travin: Processing, neural network-based modeling of biomonitoring studies data and validation on Republic of Moldova data, Proceedings of the Romanian Academy Series A-Mathematics Physics Technical Sciences Information Science; 2022, Vol. 23, No. 4, pp. 399-406
- [35] M. Stefanoni, R. Pesti, Á. Odry, and Sarcevic, P.: Measurement System for the Simulation of Indoor Magnetic Disturbances using a Robotic Arm, In 2023 IEEE 21<sup>st</sup> World Symposium on Applied Machine Intelligence and Informatics (SAMI), January 2023, pp. 000273-000278

- [36] M. Stefanoni: Repositoty of the Magnetic disturbance compensation algorithms for known objects; Available online: <https://github.com/MassimoStefanoni/magnetic-disturbance-compensation-algorithms-for-known-objects>, accessed on 12 September 2024
- [37] A. Gholamy, V. Kreinovich and O. Kosheleva: Why 70/30 or 80/20 relation between training and testing sets: A pedagogical explanation, *International Journal of Intelligent Technologies and Applied Statistics*; 2018, Vol. 11, No. 2, pp. 105-111